Downregulation of THBS2 suppresses tumorigenicity and liver metastasis of gastric cancer and increases its sensitivity to trastuzumab

Zheng-yao CHANG[1#]，Ji-Yang LI[1#], Chao ZHANG[2#], Yun-He GAO[1], Wen-Quan LIANG[1], Heng PAN[2], Ke-Cheng ZHANG[1], Jian-Xin CUI[1], Bo WEI[1], Lin CHEN[1*]& Hong-Qing XI[1*]
[*]These authors contributed equally to this work.

[1]Department of General Surgery, Chinese PLA General Hospital and Chinese PLA Medical School, Beijing 100853, China
[2]Institute for Computational Biomedicine, Weill Cornell Medicine. Department of Medicine, Division of Hematology and Medical Oncology, New York-Presbyterian Hospital, New York, NY 10021, USA

chinaXiv:202309.00234v1

[*] Corresponding author: Lin Chen(Chenlinbj@sina.com)and Hong-Qing Xi(xihongqing@126.com).

Abstract

Objective: Liver metastasis is one of the major causes of cancer-related death in gastric cancer (GC) patients. This study was to investigate the roles of THBS2 in the tumorigenesis and liver metastasis of GC and the sensitivity of GC to trastuzumab.

Methods: Sequencing was employed to identify the differentially expressed genes in the GC. The THBS2 expression was detected in GC tissues and GC cell lines, its relationships with clinicopathological characteristics were further assessed, and its roles in the malignant behaviors of GC were further investigated in vitro and in vivo, by up-regulating or down-regulating THBS2 expression. The PTEN and its downstream AKT and FAK signaling pathways were investigated in the GC aiming to explore the potential mechanism underlying the regulatory effects of THBS2.

Results: THBS2 expression increased significantly in the GC as compared to the normal gastric tissues, which was related to the distal metastasis and poor prognosis of GC patients. THBS2 expression also increased in the primary GC cells and human gastric cell line NCI-N87. THBS2 downregulation induced mesenchymal-epithelial transition (MET) and PTEN nuclear translocation, which inhibited the metastasis of GC cells. Carmofur promoted PTEN nuclear translocation, inhibiting the metastases and THBS2 downregulation together with carmofur improved the sensitivity of GC to trastuzumab.

Conclusions: THBS2 is overexpressed in GC tissues of patients with synchronous liver metastases and its overexpression is associated with poor prognosis. THBS2 downregulation inhibits the metastases of GC. THBS2 down-regulation and carmofur can be used as a new treatment for the advanced GC with metastases.

Keywords: Gastric cancer; THBS2; liver metastasis; trastuzumab

1. Introduction

Liver is the most common site of hematogenous metastasis of gastric cancer (GC) and GC patients with liver metastasis usually have a poor long-term survival[1-3]. Currently, the treatments for gastric cancer liver metastases (GCLM) are limited, and therefore understanding of pathogenesis underlying the GCLM becomes particular important. Cancer cells can escape from the control of normal cellular environment due to the continuous accumulation of genetic and epigenetic changes, and they finally form metastases. A variety of substantial oncogenes and tumor suppressor genes have been already identified in cancer tissues, including GC. However, the roles of gene dysfunction in gastric tumorigenicity are not very clear, especially in the liver metastasis of GC.

The adhesion of cells to the extracellular matrix (ECM) is crucial for the regulation of cellular morphology, migration, proliferation, survival and differentiation[4]. Abnormal ECM affects cancer progression by directly promoting cellular transformation and metastasis[5]. Focal adhesions (FAs) are large macromolecular assemblies and the primary subcellular structures that can regulate the effects of ECM adhesion on the cell behaviors[6]. This process is critical in the proliferation and migration, which is related to the tumor invasion and metastasis. Thrombospondins (THBSs) are a family of multidomain and matricellular Ca2+-binding glycoproteins released from various types of cell, including stromal fibroblasts, endothelial cells and immune cells[7]. By binding to numerous target proteins, they participate in diverse biologic processes such as tumor angiogenesis[8-12], cell motility, proliferation, adhesion, apoptosis and cytoskeletal organization, and may serve as interaction platforms in the ECM[13, 14]. THBS2 is a critical member of this family and may exert diverse biological effects by binding to ECM proteins and cell surface receptors[15]. It has been reported that THBS2 can activate integrin β1, leading to the phosphorylation of its downstream effector focal adhesion kinase (FAK)[16]. Due to its multiple functions, increasing attentions have been paid to the role of THBS2 in cancers. Currently, the role of THBS2 in the tumor formation and progression is still controversial. Some studies have reported that THBS2 is associated with tumorigenesis[17-20], but others show opposite results about the role of THBS2 in the cancer development[21-29], especially in the gastrointestinal tumor and its metastases[17, 21, 29].

In this study, the gene expression profiles of GC tissues were characterized, the roles of THBS2 in the tumorigenicity and liver metastasis of GC were further investigated in vivo and in vitro, and its effect on the sensitivity of GC to trastuzumab was explored in the GCLM xenograft model.

2. Methodology (Design/Approach)

3

2.1 Patients and GC tissues

A total of 218 GC patients with paraffin-embedded cancer tissues between January 2012 and December 2021 and 4 GC patients with fresh GC tissues, adjacent normal mucosa (at least 5 cm away from the tumor) and liver metastasized tissues between January 2016 and December 2016 were recruited from the Department of General Surgery, Chinese PLA General Hospital. The last follow-up was done in June 2021. All these patients received radical surgery without preoperative chemotherapy and/or radiotherapy. Written informed consent was provided by all participants. All specimens were handled anonymously according to the ethical standards. This study was approved by the Ethical Review Committee of our hospital. The fresh tissues were immediately frozen in liquid nitrogen and the genomic DNA and RNA were extracted as soon as possible. The paraffin-embedded tissues were all subjected to immunohistochemical staining. Pathological TNM staging was evaluated based on the Japanese Classification of Gastric Carcinoma (3rd Edition) in English[30].

2.2 Cell culture and tumorsphere formation assay

Human GC cells NCI-N87 and GES were obtained from the American Type Culture Collection Cell Biology Collection (ATCC, Manassas, VA, USA). Cells were cultured in DMEM supplemented with 10% fetal bovine serum (FBS) at 37 °C in a humidified incubator containing 5% CO_2. Primary GC cells (PGTCs) were isolated from fresh liver-metastasis tissues of GC patients and successfully grown as reported in our previous study[31] .In order to examine the pluripotent properties, PGTCs or NCI-N87 cells were cultured in ultralow attachment 24-well plates (Corning, NY, USA) at a density of 10,000 cells/ml in DMEM with 10% FBS to form spheres. Seven days later, the spheres with diameter > 100 μm were counted under a light microsphere.

2.3 Animals

Six-week-old male NOD; Scid; ll2rg–/– (NSG) mice were housed under specific pathogen-free conditions. All procedures were conducted according to the NIH guidelines and approved by the Animal Care and Use Committee of Chinese PLA General Hospital. Tissues were immediately fixed in formalin for 24 h and then embedded in paraffin.

2.4 Sequencing and data analysis

The genomic DNA and RNA were extracted from each sample and processed for library preparation and subsequent sequencing using an Illumina HiSeq 4000 platform. Each sample was sequenced as 150-bp paired-end reads. Homopolymers, adapters and distribution of base quality of raw sequences from each sample were investigated using FastQC (version 0.10.1).

2.5 GEO database

GEO_GSE77346 (Analysis of differentially expressed genes between herceptin/trastuzumab-sensitive and -resistant GC cells by transcriptome) was used for the validation of our data. We highlighted the differentially expressed genes in both our data and GEO database, and then GO analysis and regulation network analysis were performed.

2.6 Gene Set Enrichment Analysis (GSEA)

To determine whether a priori defined set of genes shows statistically significant, consistent differences between two biological states (increased expression vs. decreased expression), GSEA was performed with the JAVA program (http://softw are. Broad institute.org/gsea/downl oads.jsp) using the MSigDB C2 KEGG pathways gene sets, which contains 186 gene sets.

GSEA was performed using GSEA software (version 2.2.1). The c2.cp.kegg.v5.1.symbols.gmt dataset was obtained from the GSEA website MsigDB database. Enrichment analysis was done by default weighted enrichment statistics, with the random combinatorial count set as 1,000. Gene sets were defined as significantly enriched by $P<0.05$ as well as false discovery rates (FDR) <0.25 in the GSEA.

2.7 Machine-learning algorithm

The Gradient Boosting Decision Tree (GBDT) model, a type of ensemble machine learning algorithm which can build binary classification prediction model, was used to identify the risk factors associated with short postoperative survival (less than 5 years). GBDT model trains many base decision trees in a gradual, additive and sequential manner. In m-th step, GBDT fits a single decision tree to pseudo-residuals of single decision trees of (m-1)-th step. Then, all the single trees were ensembled in order to achieve a better classification performance. Although GBDT is good at fitting training samples, it has a risk of overfitting. To avoid this disadvantage, following hyper-parameters were used: max_depth = 8 (limit the max depth of each decision tree as 8), min_child_weight = 7.4022 (minimum sum of sample weight needed in a leaf node of single decision tree), subsample = 0.866 (randomly select 86.6% training samples to train a single decision tree), colsample_bytree = 0.501 (randomly select 50.1% features to train a single decision tree). In this way, the generalization power of the prediction model and the accuracy of overall variable importance were improved. Variable importance identifies the most important variables based on their contribution to the predictive accuracy of the model[32].

2.8 Immunohistochemical and H&E staining

Sections (5 μm in thickness) were obtained from paraffin-embedded human or mouse tissues. Then, the sections were blocked with 3% H_2O_2 in methanol and subsequently incubated with anti-THBS2 (Abcam, ab84469) at 4°C overnight. For negative controls, the primary antibodies were replaced with normal rabbit serum. H&E staining was performed for histological assay. The sections were observed

under the Olympus BX-UCB light-field microscope, and 5 fields were randomly selected at ×400 for assay. The immunoreactivity score (IRS) was determined independently by two authors (Y.G. and H.X.), based on the staining intensity and percentage of positive cells. Staining intensity was scored as follows: 0, no staining; 1+, weak staining; 2+, moderate staining; and 3+, strong staining. The percentage of positive cells was scored as follows: 0, no positive cells; 1+, up to 25% of positive cells; 2+, 25–75% of positive cells; and 3+, >75% of positive cells. The IRS was the multiplication of both scores (IRS 0-9) and classified as negative (IRS = 0-2) and positive (IRS = 3-9).

2.9 Gene silencing, overexpression and cell transfection

For construction of plasmids, three shRNA sequences targeting THBS2 were cloned into PLK vector for lentivirus packaging (Genechem Co. Ltd., Shanghai, China). The full coding sequence of THBS2 was cloned into GV492 vector for overexpression. The primers used for THBS2 knockdown or overexpression are shown in the Supplementary Table 1.

For lentivirus packaging, the core plasmids were co-transfected with the packaging plasmids into 293T cells. The calcium phosphate co-precipitation method was used, and the medium was refreshed 12 h post-transfection. The supernatants containing virus were collected at 48 h and filtered through a 0.45-μm membrane, and then the virus was concentrated by centrifugation at 55,000×g for 120 min at 4 °C. The pellet was resuspended, aliquoted, and stored at −80°C.

For cell transfection, cells were grown to 70% confluence in 6-well plates and then transfected with virus in the presence of 5 μg/ml polybrene. The medium was refreshed 24 h later. Next, the cells were transferred into 10-cm dishes and screened with puromycin or G418 (ab144261, Abcam, MA, USA) for at least 6-8 weeks before experiments.

2.10 Real-time Quantitative PCR

Total RNA from cells was extracted using Trizol reagent (Invitrogen) according to the manufacturer's instructions. First-strand cDNA was synthesized using HiScriptQ RT SuperMix for qPCR (Vazyme, Nanjing, China). Quantitative real-time PCR was performed using AceQ SYBR Master Mix (Vazyme, Nanjing, China) on an ABI 7900HT Sequence Detection System (Applied Biosystems, CA, USA). The PCR primers used to amplify target genes are shown in Supplementary Table 2. GAPDH served as the internal reference. Each sample was tested in triplicate.

2.11 Protein extraction and Western blotting

Nuclear protein and cytoplasmic protein were extracted according to the manufacturer's instructions (Nuclear-Cytosol Extraction Kit #P1200, Applygen, Beijing, China). The protein concentration was determined with BCA assay Kit (Bio-Rad). The primary antibodies were as follows: anti-THBS2 antibody (Abcam, ab84469), anti-PTEN antibody (CST, #9188), anti-pPTEN antibody (CST, #9551s),

anti-FAK antibody (CST, #3285), anti-pFAK antibody (CST, #3281), anti-AKT antibody (CST, #2920), anti-pAKT antibody (CST, #4060), anti-E-cadherin (Abcam, ab15148), anti-Vimentin antibody (CST, #5741), anti-N-cadherin antibody (CST, #8480), anti- PBK antibody (CST, #4942), anti-STMN1 antibody (CST, # 4191s), anti-β-actin antibody (CST, #3700), anti-tubulin antibody (CST, #5666), anti-lamin b1 antibody (CST, #13435), and anti-GAPDH antibody (CST, # 5174). The protein bands were visualized using the Tanon-5200 Image Analyzer. Paired mean comparisons were performed to assess concentration-dependent changes in the intensity of native protein bands. The relative expression of protein was calculated by normalizing target protein to β-actin (internal reference). All experiments were repeated at least three times under the same conditions. The representative images were captured and analyzed. Data are expressed as mean ± standard deviation (SD; n=3).

2.12 Cell scratch test

When cell confluence reached about 100%, a scratch was made using a sterile 200-μL pipette tip. The initial distance between wounds was recorded (0 h) by photographing under an inverted microscope at 100×. The wound distance was then recorded at 24 h and 48 h, and the relative migration rate of cells was calculated. The width of the scratch was analyzed using the Image J software. All experiments were repeated at least three times under the same conditions. The representative images were captured and analyzed. Data are presented as mean ± SD (n=3).

2.13 Trastuzumab sensitivity assay

Trastuzumab (Herceptin) was kindly provided by Roche Pharma (Shanghai, China) for nonclinical investigations. PGTCs treated with 3 mM Carmofur (M2247, AbMole) or DMSO (control group) for 48 h; NCI-N87 cells treated with 5 mM Carmofur or DMSO for 48 h were seeded at a density of 5000 cells per well in 96-well plates. Then, all these cells were treated with Herceptin at different concentrations (0, 1, 2, 3, 4, 5 and 10 μg/ml) for 72 h. The Cell Counting Kit-8 (CCK-8; Dojindo, Kumamoto, Japan) was used to examine the survival rate of these cells. Cells in each well were incubated with 10 μl of CCK-8 solution for 60 min at 37 °C in dark. Viable cells were examined by measuring the absorbance at 450 nm.

2.14 Orthotopic xenograft assay

All procedures were performed aseptically to ensure recovery after implantation. After intraperitoneal anesthesia (Avertin, T48402, Sigma-Aldrich), a 1-cm incision was longitudinally made right below the xyphoid of a NSG mouse. About 1×10^6 cells were injected into the gastric serosa of NSG mice. Twenty-four mice (6 for each group) were treated with four types of cancer cells: PGTCs, PGTCsTHBS2-, NCI-N87 and NCI-N87THBS2+. After one-week postoperative recovery, mice in

each group were randomly divided into carmofur group (n=3) and control group (n=3). Carmofur (10 mg/kg) or sterile saline solution was administrated intragastrically once every two days for 18 weeks. At the end of treatment, mice were sacrificed and the tumors and metastases were assessed.

2.15 Subcutaneous xenograft assay

$5×10^6$ cells mixed with matrigel (Corning) at a ratio of 1:1 (200 μl per mouse) were subcutaneously injected into the rear flank of NSG mice. Eighteen mice (12 in each group) were injected with either PGTCs or NCI-N87 cells. Two weeks later, the tumors (about 200 mm3) became palpable and measurable, and then treatments were initiated. Mice in each group were randomly divided into four groups: control group (n=3), carmofur group (n=3), Herceptin group (n=3) and carmofur + Herceptin group (n=3). In the next 6 weeks, carmofur (10 mg/kg) was administrated intragastrically once every two days; Herceptin (10 mg/kg) was injected intraperitoneally twice weekly in corresponding groups. Sterile saline solution was used in the control group. Tumor diameters were measured using a vernier caliper every week and the tumor volume (V) was calculated as follow: V (mm3) = 0.5 × length × width^2.

2.16 Statistical analysis

Continuous variables are expressed as mean ± SD, normal distribution was tested using the one-sample Kolmogorov–Smirnov test and comparisons were done with Student's t-test or Kruskal-Wallis test. Binomial and categorical data were compared using Pearson's χ2 or two-tailed Fisher's exact test, while analysis of variance (ANOVA) was employed for comparisons among multiple groups. Overall survival curves were estimated using the Kaplan–Meier method, and the survival was analyzed using the log-rank test. A value of P<0.05 was considered statistically significant. The GraphPad Prism software statistical package and statistical software package R (http://www.R-project.org; The R Foundation) and Empower States (http://www.empowerstates.com; X & Y Solutions, Inc., Boston, MA, USA) were used for statistical analyses.

3. Results

3.1 THBS2 is involved in GC metastasis.

DEGs were examined in GC tissues as compared to normal samples. In order to confirm our findings, the DEGs were detected in 31 matched normal and tumor samples from TCGA as well. 555 common DEGs between our samples and TCGA were detected for downstream pathway enrichment analysis in the KEGG database. About 555 genes related to the ECM-receptor interaction pathways and focal adhesion (FA) pathways were significantly overexpressed (Fig. 1a). A group of genes which are involved in ECM-receptor interaction and FA pathways were significantly up-regulated in the GC

tissues, including THBS2, SPP1, HGF, ITGA2, LAMC2, COL1A1, COL1A2 and so on (Fig. S1). All these genes have been reported to be associated with tumorigenesis and metastasis in multiple cancer studies[33-37], but the mechanism by which ECM components promote GC metastasis is still unclear. Among these up-regulated genes in the ECM/FA pathways, we focused on THBS2 because it is closely related to GC metastasis.

As an adhesive glycoprotein, THBS2 expression is significantly down-regulated in all digestive tract organs (Fig. 1b, Fig. S2). In the present study, the THBS2 expression was markedly up-regulated in the GC tissues as compared to normal tissues in both our samples and TCGA study (Fig. 1c). Moreover, the expression of THBS2 was higher in M1 tissues in TCGA vs N0 (M0) and N3 (M0), which indicates the potential role of THBS2 in the hematogenous metastasis of GC (Fig. 1d).

3.2 THBS2 expression is significantly associated with prognosis of GC patients.

To explore the clinical importance of THBS2 in GC, immunohistochemical (IHC) staining was performed to assess the protein expression of THBS2 with immunoreactivity score (IRS) (Fig. 2a). The poorly differentiated GC tissues tended to have the strongest staining. As shown in Fig. 2b, patients with higher THBS2 expression had significantly shorter overall survival time, whereas patients with lower THBS2 expression had a favorable prognosis (median 28.5 vs. 40.5 months, P = 0.00039). The relationship between THBS2 expression and clinicopathological characteristics was further investigated in the THBS2-positive and negative groups (Table 1). The proportion of poor or signet-ring differentiation patients in the THBS2+ group was significantly higher than in the THBS2- group (83.3% vs. 67.4%, P=0.012). There were more patients with stage N3 GC (59.1% vs 37.2%, P=0.018) and hematogenous metastases (12.1% vs 3.5%, P=0.028) in the THBS2+ group than in the THBS2- group.

3.3 THBS2 downregulation in PGTCs inhibits EMT though both FAK and AKT signaling pathways

The passage number of PGTCs is expressed as P. Number. The P1, P3, P6 and P10 PGTC are shown in Fig. 3a. THBS-2 protein expression in the PGTCs was relatively higher than in the GES cells, while PTEN protein expression was comparable between two cell types (Fig.3b). To understand the biological roles of THBS2 in the GCLM, the THBS2 expression was knocked down in the PGTCs. Results showed the THBS2 expression reduced by 80%, and then these cells were named PGTCsTHBS2-. Further analysis showed the downregulation of THBS2 expression failed to alter the PTEN expression, but suppressed the pPTEN expression and inhibited the activation of AKT and FAK signaling pathways (Fig. 3c and 3d).

As shown in Fig. 3e, downregulation of THBS2 expression tended to increase the expression of epithelial marker E-cadherin, but decreased the expression of mesenchymal makers Vimentin and N-cadherin, which implies that the PGTCsTHBS2- might be involved in the mesenchymal-epithelial transition (MET). Cell scratch test showed PGTCs migrated significantly faster than PGTCsTHBS2- (Fig. 3f). In addition, the tumorispheres generated by PGTCs were more than 5.4 times that generated by PGTCsTHBS2- (Fig. 3g). Our results indicated that down-regulation of THBS2 expression induced MET of GCLM cells which exerted less migrating and stemness properties and became non-metastatic.

3.4 THBS2 overexpression in NCI-N87 cells regulates cell division, cell cycle, phosphorylation, movement of cell or subcellular components and activates PTEN phosphorylation

The heat map showed the cluster of DEGs in the transcriptome and proteome data (Fig. 4a and b). The numbers of DEGs between proteome, transcriptome and GEO database are shown in the Venn diagram (Figure 4c), which exhibits the relationship between THBS2 and trastuzumab sensitivity from our data and GEO database. GSEA revealed the global transcriptome differences in main biological processes after THBS2 overexpression in NCI-N87 cells, and these were related to cell division, cell cycle, phosphorylation, movement of cell and subcellular component (Figure 4d). Regulation network diagram was constructed using the DEGs obtained by combining the transcriptome, proteome and GEO data (Figure 4e). Furthermore, Western blotting was conducted to confirm the expression of key proteins in this regulation network (Figure 4f). Results showed that PTEN phosphorylation was activated after THBS2 overexpression. The phosphorylation of PTEN leads to its inactivation, and therefore tumor inhibition of PTEN reduces.

3.5 Carmofur increases sensitivity of PGTCs and NCI-N87 cells to trastuzumab

PTEN protein tends to express in the cytoplasm,but not the nucleus of PGTCs and NCI-N87 cells (Figure. 5a). Figure. 5b showed that carmofur altered the subcellular location of PTEN in vitro. When cell confluence reached 70%-80%, cells were incubated with carmofur at different concentrations (0,1,3,5 and 10 mM). After 48-h incubation, the protein expression of nuclear and cytoplasm PTEN was detected. Results showed the most effective concentrations at which carmofur exerted the best inhibitory effect on the proliferation of PGTCs and NCI-N87 cells were 3 mM and 5 mM, respectively. Cells treated with carmofur at optimal concentrations for at least 48 h were named PGTCs/carmofur or NCI-N87/carmofur. PGTCs and NCI-87 cells were both HER2-positive cells (Fig. S3). The sensitivity to trastuzumab was assessed in cells with or without carmofur treatment. As shown in Fig. 5c,the cut-off concentration of trastuzumab in the PGTCs/carmofur group occurred earlier than in the PGTCs group (4 μg/ml vs 5 μg/ml). Similar result was noted in the NCI-N87/carmofur cells compared with NCI-N87 cells (3 μg/ml vs 5 μg/ml). Carmofur treatment also reduced the tumorispheres in two cell lines as compared to Carmofur-free cell lines (Fig. 5d).

3.6 THBS2 and carmofur synergistically sensibilize GC to trastuzumab in vivo

The effect of THBS2 and carmofur treatment on the GC was further investigated in orthotropic xenograft model (Fig. 6a). All mice had tumors in the stomach after they were sacrificed at the end of the 19th week. Liver metastases were only noted in the high THBS2 expression group: 2 out of 3 in the PGTCs group and 1 out of 3 in the NCI-N87THBS2+ group. Neither THBS2 knock-down nor carmofur treated groups had liver metastases. In addition, the liver metastases were identified under the light microscope after H&E staining. To explore the sensitivity of GC to trastuzumab after THBS2 down-regulation and carmofur treatment, subcutaneous xenograft model was established in mice. In the NCI-N87 group, carmofur treatment significantly reduced the tumor volume from 475 mm3 in the control group to 290 mm3 (38.95% reduction), and trastuzumab treatment reduced the tumor volume by 62.11% (from 475 mm3 to 180 mm3). The combined treatment of carmofur and trastuzumab

achieved the best tumor-inhibitory effect, and the tumor volume reduced by 93.26% (from 475 mm3to 32 mm3) (Fig. 6b). While in the NCI-N87THBS2+ group (Fig. 6c), carmofur failed to significantly reduce the tumor volume (750 mm3 vs 620 mm3, P=0.479). Trastuzumab still markedly reduced the tumor volume from 750 mm3 in the control group to 230 mm3 (69.33% reduction), but the combination of trastuzumab and carmofur failed to further significantly reduced the tumor volume (230 mm3 in trastuzumab group vs 80 mm3 in trastuzumab and carmofur group, P=0.052). Furthermore, the final tumor volume (8th week) was examined in two groups (Fig. 6d). Results showed that the tumor volume in the NCI-N87 group was significantly smaller than in the NCI-N87THBS2+ group.

4. Discussion

THBS2 is involved in ECM-receptor interaction and FA pathways, and its expression was significantly up-regulated in the GC tissues. THBS2 expression was higher in patients with lymph node and hematogenous metastases and associated with shorter overall survival time. Downregulation of THBS2 in the PGTCs inhibited EMT though both FAK and AKT signaling pathways. THBS2 overexpression in the NCI-N87 cells regulated cell division, cell cycle, phosphorylation, movement of cells and subcellular component and activated the phosphorylation of PTEN, compromising the tumor inhibitory effect of PTEN. Carmofur increased sensitivity of PGTCs and NCI-N87 cells to trastuzumab. THBS2 and carmofur exerted synergistic effect on the sensitivity of GC cells to trastuzumab in the xenograft model.

In our study, THBS2 was overexpressed in GC tissues from patients with synchronous liver metastases, which was associated with a poor prognosis. In addition, higher THBS2 expression in stage M1 samples in TCGA vs N0 (M0) and N3 (M0) samples, which indicates the potential role of THBS2 in the hematogenous metastasis of GC. Furthermore, the machine-learning algorithm model was employed to quantify the relative importance of THBS2 to the postoperative long-term survival in GC patients. It has been reported that machine learning algorithm is more accurate than traditional logistic regression[38, 39], including the ability to recognize clinically important risk among patients with several marginal risk factors and continually incorporate new clinical data with minimal oversight32.

In the investigation of mechanism underlying the role of THBS2 in the GC, we focused on the phosphatase and tensin homologue (PTEN), a tumor suppressor[40], due to its association with the development of metastases in the last phase of tumor progression[41]. PTEN functions as a PIP3 phosphatase and is the main negative regulator of PI3K-Akt pathway and a regulator of switch between cell proliferation and migration states[42]. After down-regulation of THBS2 expression, PTEN was activated and AKT was inhibited. Considering the interaction between PTEN and FAK in the

11

GC[43], the expression of FAK was further tested. Consistent with previous studies, PTEN also affected the oncogenic pathways besides the PI3K-Akt pathway, such as PTEN/FAK. Based on the available findings[44], we speculate that PTEN may reduce tyrosine phosphorylation of FAK, and in turn the regulation of FAK partially antagonizes the effects of PTEN. In line with previous findings16, THBS2 can activate integrin β1 and phosphorylate its downstream effector FAK, which is a main regulator of ECM6. PTEN may function as a tumor suppressor by negatively regulating cell interactions with ECM[45]. Therefore, we speculate that THBS2 may serve as a target gene based on concomitant regulation of PI3K/AKT and FAK signaling.

One of the most important processes in tumor metastases and distant colonization is the MET, in which the epithelial program is restored by repressing the mesenchymal program. On the other hand, epithelial cancer cells must undergo EMT, which allows them to migrate from primary lesions to distant organs [46]. After down-regulation of THBS2 expression, cells tend to undergo MET process which is an essential process when the tumor cells become less migratory and invasive.

GSEA analysis was performed to further investigate the potential role of THBS2 in the GC. In order to exclude the particularity of PGTCs, NCI-N87 cells were used to overexpress THBS2. GSEA analysis showed that global transcriptome differences after THBS2 overexpression were mainly found in the phosphorylation and movement of cell or subcellular component processes.

Binding to ITGA1 is a requisite step in the functioning of THBS2[47]. They were both differentially expressed in the breast cancer[48]. PBK can directly interact with, phosphorylate and inactivate PTEN, which in turn activates PI3K-Akt-IKK signaling pathway[49, 50].PBK-induced cell migration has been found to be a PI3K/AKT-dependent event[51], and PBK overexpression is also closely related to venous invasion, tumor depth and recurrence rate of GC[52]. STMN1 is one of the genes down-regulated upon PTEN induction and an accurate IHC marker of the signature and has prognostic significance in the breast cancer[53]. STMN1 is an important member of PI3K pathway[54]. STMN1 overexpression is significantly associated with the lymphatic metastatic recurrence in pN0 ESCC patients. STMN1 expression is regulated by the PI3K pathway, and STMN1 can act as a surrogate marker of PI3K signaling pathway related to tumor recurrence[55]. In our study, THBS2 overexpression activates the PI3K signaling pathway by inactivating PTEN. Therefore, regulation of THBS2 or PTEN may be an important strategy to increase the sensitivity of GC to trastuzumab.

Trastuzumab (Herceptin; Genentech, San Francisco, Calif., USA) is a recombinant, humanized monoclonal antibody targeting the extracellular domain of the human epidermal growth factor receptor 2 (HER2) protein. It is the first biological product that can prolong the survival time of metastatic GC patients[56]. In EU and US, trastuzumab combined with chemotherapy has been approved by the FDA as first-line treatment for metastatic GC with Her-2 over-expression. Despite early successes, the majority of patients exhibit primary or secondary resistance within one year, which severely influences the clinical application of trastuzumab. The trastuzumab resistance has also

been reported in the treatment of metastatic breast cancer[57]. Thus, to develop appropriate chemo-sensitizers according to potential mechanisms related to trastuzumab resistance may be important for the clinical application of trastuzumab. The activation of PTEN/PI3K/AKT signaling pathway is one of the major mechanisms leading to the resistance of GC cells to trastuzumab[58]. Therefore, PTEN as a molecule in the PI3K pathway has been identified as an important target in studies on the treatment of cancers[59-61]. One of the alternative targets of PTEN is the FAK kinase, which is mainly involved in the control of cancer cell spread[41]. Therefore, we speculated that THBS2 may serve as a key factor that can regulate PI3K and FAK signaling pathways to improve the trastuzumab resistance.

Carmofur (1-hexylcarbamoyl-5-fluorouracil, HCFU) has been used as oral drug in the chemotherapy of advanced gastrointestinal cancer[62, 63] and advanced pancreatic cancer[64] in the early nineties. Studies have confirmed its preventive effect on distant metastases[65, 66]. In our study, carmofur was found to induce PTEN nuclear translocation and made the cut-off point of trastuzumab concentration-effect appeared ahead of time. In normal tissues, PTEN is localized primarily in the nucleus, whereas, in the neoplastic tissues, PTEN translocates into cytoplasm, which may be involved in the neoplastic transformation[67].

Several mechanisms have been proposed for the nucleo-cytoplasmic translocation of PTEN, including simple diffusion, cytoplasmic localization signal mediated translocation, active translocation mediated by the RAN GTPase or major vault protein, phosphorylation-dependent translocation and monoubiquitylation-dependent translocation[67]. As THBS2 over-expression is enriched in the phosphorylation process, the phosphorylation-dependent translocation may be a feasible theory for the PTEN nucleo-cytoplasmic translocation proposed by Vazquez et al [68]. Carmofur alone as an adjuvant chemotherapy is not sufficient to improve the prognosis[69] and its clinical utility is also limited due to its possible toxic leukoencephalopathy [70]. However, our study shed new light on carmofur as a potential chemo-sensitizer to trastuzumab based on its ability to induce PTEN nuclear translocation. Therefore, we investigated the effect of carmofur combined with THBS2 down-regulation as a new strategy to enhance the sensitivity of GC to trastuzumab in the xenograft model. In orthotropic xenograft model, liver metastases were only noted in the high THBS2 expression group: 2 out of 3 in the PGTCs group and 1 out of 3 in the NCI-N87THBS2+ group. Neither THBS2 knock-down nor carmofur treated groups had liver metastases. In the subcutaneous xenograft model, the effect of THBS2 knock-down combined with carmofur on the sensitivity of NCI-N87 cells to trastuzumab was further explored. Results indicated that carmofur increased the sensitivity of GC to trastuzumab in the NCI-N87 group.

13

5. Conclusion

Taken together, our study indicates THBS2 is overexpressed in the GC tissues of patients with synchronous liver metastases, which is associated with the poor prognosis of GC. In addition, high THBS2 expression promotes EMT and metastases of GC, which may be related to classic AKT and FAK signaling pathways. Moreover, THBS2 downregulation combined with carmofur may serve as a new strategy to enhance the sensitivity of GC to trastuzumab.

ACKNOWLEDGEMENTS

Supplementary Materials

Figure S1. Expressions of genes involved in ECM-receptor interaction and FA pathways, including SPP1, HGF, ITGA2, LAMC2, COL1A1, and COL1A2, in the GC tissues among the TCGA samples and our samples.

Figure S2. THBS2 expression is significantly down-regulated in all digestive tract organs.

Figure S3. WB results of HER2 expressions in PGTCs and NCI-87 cells.

Table S1. Primers' information used for THBS2 knockdown or overexpression.

Table S2. Primers' information used for PCR.

chinaXiv:202309.00234v1

References

[1] Yamada Y, Higuchi K, Nishikawa K, Gotoh M, Fuse N, Sugimoto N, et al. Phase III study comparing oxaliplatin plus S-1 with cisplatin plus S-1 in chemotherapy-naive patients with advanced gastric cancer. Ann Oncol. 2015;26(1):141-8.

[2] Shah MA. Update on metastatic gastric and esophageal cancers. J Clin Oncol. 2015;33(16):1760-9.

[3] Tatsubayashi T, Tanizawa Y, Miki Y, Tokunaga M, Bando E, Kawamura T, et al. Treatment outcomes of hepatectomy for liver metastases of gastric cancer diagnosed using contrast-enhanced magnetic resonance imaging. Gastric Cancer. 2017;20(2):387-93.

[4] Nagano M, Hoshino D, Koshikawa N, Akizawa T, Seiki M. Turnover of focal adhesions and cancer cell migration. Int J Cell Biol. 2012;2012:310616.

[5] Lu P, Weaver VM, Werb Z. The extracellular matrix: a dynamic niche in cancer progression. J Cell Biol. 2012;196(4):395-406.

[6] Chen CS, Alonso JL, Ostuni E, Whitesides GM, Ingber DE. Cell shape provides global control of focal adhesion assembly. Biochem Biophys Res Commun. 2003;307(2):355-61.

[7] Bornstein P. Thrombospondins function as regulators of angiogenesis. Journal of cell communication and signaling. 2009;3(3-4):189-200.

[8] Iruela-Arispe ML, Luque A, Lee N. Thrombospondin modules and angiogenesis. The international journal of biochemistry & cell biology. 2004;36(6):1070-8.

[9] Lawler PR, Lawler J. Molecular basis for the regulation of angiogenesis by thrombospondin-1 and -2. Cold Spring Harbor perspectives in medicine. 2012;2(5):a006627.

[10] Folkman J. Tumor angiogenesis: therapeutic implications. The New England journal of medicine. 1971;285(21):1182-6.

[11] Ferrara N, Kerbel RS. Angiogenesis as a therapeutic target. Nature. 2005;438(7070):967-74.

[12] Carmeliet P, Jain RK. Angiogenesis in cancer and other diseases. Nature. 2000;407(6801):249-57.

[13] Stenina OI, Topol EJ, Plow EF. Thrombospondins, their polymorphisms, and cardiovascular disease. Arteriosclerosis, thrombosis, and vascular biology. 2007;27(9):1886-94.

[14] Adams JC, Lawler J. The thrombospondins. The international journal of biochemistry & cell biology. 2004;36(6):961-8.

[15] Bornstein P, Armstrong LC, Hankenson KD, Kyriakides TR, Yang Z. Thrombospondin 2, a matricellular protein with diverse functions. Matrix biology : journal of the International Society for Matrix Biology. 2000;19(7):557-68.

[16] Del Pozo Martin Y, Park D, Ramachandran A, Ombrato L, Calvo F, Chakravarty P, et al. Mesenchymal Cancer Cell-Stroma Crosstalk Promotes Niche Activation, Epithelial Reversion, and Metastatic Colonization. Cell Rep. 2015;13(11):2456-69.

[17] Yang S, Shin J, Park KH, Jeung HC, Rha SY, Noh SH, et al. Molecular basis of the differences between normal and tumor tissues of gastric cancer. Biochim Biophys Acta. 2007;1772(9):1033-40-.

[18] Lin CY, Lin CY, Chang IW, Sheu MJ, Li CF, Lee SW, et al. Low thrombospondin 2 expression is predictive of low tumor regression after neoadjuvant chemoradiotherapy in rectal cancer. Am J Transl Res. 2015;7(11):2423-32.

[19]   Zubor P, Hatok J, Moricova P, Kajo K, Kapustova I, Mendelova A, et al. Gene expression abnormalities in histologically normal breast epithelium from patients with luminal type of breast cancer. Molecular biology reports. 2015;42(5):977-88.

[20]   Tian ZQ, Li ZH, Wen SW, Zhang YF, Li Y, Cheng JG, et al. Identification of Commonly Dysregulated Genes in Non-small-cell Lung Cancer by Integrated Analysis of Microarray Data and qRT-PCR Validation. Lung. 2015;193(4):583-92.

[21]   Tokunaga T, Nakamura M, Oshika Y, Abe Y, Ozeki Y, Fukushima Y, et al. Thrombospondin 2 expression is correlated with inhibition of angiogenesis and metastasis of colon cancer. British journal of cancer. 1999;79(2):354-9.

[22]   Koch M, Hussein F, Woeste A, Grundker C, Frontzek K, Emons G, et al. CD36-mediated activation of endothelial cell apoptosis by an N-terminal recombinant fragment of thrombospondin-2 inhibits breast cancer growth and metastasis in vivo. Breast Cancer Res Treat. 2011;128(2):337-46-.

[23]   Oshika Y, Masuda K, Tokunaga T, Hatanaka H, Kamiya T, Abe Y, et al. Thrombospondin 2 gene expression is correlated with decreased vascularity in non-small cell lung cancer. Clin Cancer Res. 1998;4(7):1785-8-.

[24]   Chijiwa T, Abe Y, Inoue Y, Matsumoto H, Kawai K, Matsuyama M, et al. Cancerous, but not stromal, thrombospondin-2 contributes prognosis in pulmonary adenocarcinoma. Oncology reports. 2009;22(2):279-83.

[25]   Weng TY, Wang CY, Hung YH, Chen WC, Chen YL, Lai MD. Differential Expression Pattern of THBS1 and THBS2 in Lung Cancer: Clinical Outcome and a Systematic-Analysis of Microarray Databases. PLoS One. 2016;11(8):e0161007.

[26]   Rendtlew Danielsen JM, Knudsen LM, Dahl IM, Lodahl M, Rasmussen T. Dysregulation of CD47 and the ligands thrombospondin 1 and 2 in multiple myeloma. British journal of haematology. 2007;138(6):756-60.

[27]   Chijiwa T, Abe Y, Ikoma N, Yamazaki H, Tsukamoto H, Suemizu H, et al. Thrombospondin 2 inhibits metastasis of human malignant melanoma through microenvironment-modification in NOD/SCID/gammaCnull (NOG) mice. Int J Oncol. 2009;34(1):5-13-.

[28]   Matos AR, Coutinho-Camillo CM, Thuler LC, Fonseca FP, Soares FA, Silva EA, et al. Expression analysis of thrombospondin 2 in prostate cancer and benign prostatic hyperplasia. Exp Mol Pathol. 2013;94(3):438-44-.

[29]   Sun R, Wu J, Chen Y, Lu M, Zhang S, Lu D, et al. Down regulation of Thrombospondin2 predicts poor prognosis in patients with gastric cancer. Mol Cancer. 2014;13:225-.

[30]   Japanese Gastric Cancer A. Japanese classification of gastric carcinoma: 3rd English edition. Gastric Cancer. 2011;14(2):101-12.

[31]   Gao Y, Cai A, Xi H, Li J, Xu W, Zhang Y, et al. Ring finger protein 43 associates with gastric cancer progression and attenuates the stemness of gastric cancer stem-like cells via the Wnt-beta/catenin signaling pathway. Stem cell research & therapy. 2017;8(1):98.

[32]   Singal AG, Mukherjee A, Elmunzer BJ, Higgins PD, Lok AS, Zhu J, et al. Machine learning algorithms outperform conventional regression models in predicting development of hepatocellular carcinoma. Am J Gastroenterol. 2013;108(11):1723-30.

[33]   Ao R, Guan L, Wang Y, Wang JN. Silencing of COL1A2, COL6A3, and THBS2 inhibits gastric cancer cell proliferation, migration, and invasion while promoting apoptosis through the PI3k-Akt signaling pathway. J Cell Biochem. 2017.

[34]   Wai PY, Kuo PC. The role of Osteopontin in tumor metastasis. J Surg Res. 2004;121(2):228-41.

[35]   Li Y, Guessous F, DiPierro C, Zhang Y, Mudrick T, Fuller L, et al. Interactions between PTEN and the c-Met pathway in glioblastoma and implications for therapy. Mol Cancer Ther. 2009;8(2):376-85.

[36]   Yang Q, Bavi P, Wang JY, Roehrl MH. Immuno-proteomic discovery of tumor tissue autoantigens identifies olfactomedin 4, CD11b, and integrin alpha-2 as markers of colorectal cancer with liver metastases. Journal of proteomics. 2017;168:53-65.

[37]   Moon YW, Rao G, Kim JJ, Shim HS, Park KS, An SS, et al. LAMC2 enhances the metastatic potential of lung adenocarcinoma. Cell Death Differ. 2015;22(8):1341-52.

[38]   Le Gall JR, Lemeshow S, Saulnier F. A new Simplified Acute Physiology Score (SAPS II) based on a European/North American multicenter study. JAMA. 1993;270(24):2957-63.

[39]   Churpek MM, Yuen TC, Winslow C, Meltzer DO, Kattan MW, Edelson DP. Multicenter Comparison of Machine Learning Methods and Conventional Regression for Predicting Clinical Deterioration on the Wards. Crit Care Med. 2016;44(2):368-74.

[40]   Lu Y, Lin YZ, LaPushin R, Cuevas B, Fang X, Yu SX, et al. The PTEN/MMAC1/TEP tumor suppressor gene decreases cell growth and induces apoptosis and anoikis in breast cancer cells. Oncogene. 1999;18(50):7034-45.

[41]   Alfieri R, Giovannetti E, Bonelli M, Cavazzoni A. New Treatment Opportunities in Phosphatase and Tensin Homolog (PTEN)-Deficient Tumors: Focus on PTEN/Focal Adhesion Kinase Pathway. Front Oncol. 2017;7:170.

[42]   Georgescu MM. PTEN Tumor Suppressor Network in PI3K-Akt Pathway Control. Genes Cancer. 2010;1(12):1170-7.

[43]   Zhang LL, Liu J, Lei S, Zhang J, Zhou W, Yu HG. PTEN inhibits the invasion and metastasis of gastric cancer via downregulation of FAK expression. Cell Signal. 2014;26(5):1011-20.

[44]   Tzenaki N, Aivaliotis M, Papakonstanti EA. Focal adhesion kinase phosphorylates the phosphatase and tensin homolog deleted on chromosome 10 under the control of p110delta phosphoinositide-3 kinase. FASEB J. 2015;29(12):4840-52.

[45]   Tamura M, Gu J, Matsumoto K, Aota S, Parsons R, Yamada KM. Inhibition of cell migration, spreading, and focal adhesions by tumor suppressor PTEN. Science. 1998;280(5369):1614-7.

[46]   Lamouille S, Xu J, Derynck R. Molecular mechanisms of epithelial-mesenchymal transition. Nat Rev Mol Cell Biol. 2014;15(3):178-96.

[47]   Chanana B, Graf R, Koledachkina T, Pflanz R, Vorbruggen G. AlphaPS2 integrin-mediated muscle attachment in Drosophila requires the ECM protein Thrombospondin. Mech Dev. 2007;124(6):463-75.

[48]   Sun Z, Wang CY, Lawson DA, Kwek S, Velozo HG, Owyong M, et al. Single-cell RNA sequencing reveals gene expression signatures of breast cancer-associated endothelial cells. Oncotarget. 2018;9(13):10945-61.

[49]   Shinde SR, Gangula NR, Kavela S, Pandey V, Maddika S. TOPK and PTEN participate in CHFR mediated mitotic checkpoint. Cellular signalling. 2013;25(12):2511-7.

[50]   Ishikawa C, Senba M, Mori N. Mitotic kinase PBK/TOPK as a therapeutic target for adult T?cell leukemia/lymphoma. International journal of oncology. 2018;53(2):801-14.

[51]   Shih MC, Chen JY, Wu YC, Jan YH, Yang BM, Lu PJ, et al. TOPK/PBK promotes cell migration via modulation of the PI3K/PTEN/AKT pathway and is associated with poor prognosis in lung cancer. Oncogene. 2012;31(19):2389-400.

[52]   Ohashi T, Komatsu S, Ichikawa D, Miyamae M, Okajima W, Imamura T, et al. Overexpression of PBK/TOPK relates to tumour malignant potential and poor outcome of gastric carcinoma. British journal of cancer. 2017;116(2):218-26.

[53]   Saal LH, Johansson P, Holm K, Gruvberger-Saal SK, She QB, Maurer M, et al. Poor prognosis in carcinoma is associated with a gene expression signature of aberrant PTEN tumor suppressor pathway activity. Proceedings of the National Academy of Sciences of the United States of America. 2007;104(18):7564-9.

[54]   Salvesen HB, Carter SL, Mannelqvist M, Dutt A, Getz G, Stefansson IM, et al. Integrated genomic profiling of endometrial carcinoma associates aggressive tumors with indicators of PI3 kinase activation. Proceedings of the National Academy of Sciences of the United States of America. 2009;106(12):4834-9.

[55]   Jiang W, Huang S, Song L, Wang Z. STMN1, a prognostic predictor of esophageal squamous cell carcinoma, is a marker of the activation of the PI3K pathway. Oncology reports. 2018;39(2):834-42.

[56]   Bang YJ, Van Cutsem E, Feyereislova A, Chung HC, Shen L, Sawaki A, et al. Trastuzumab in combination with chemotherapy versus chemotherapy alone for treatment of HER2-positive advanced gastric or gastro-oesophageal junction cancer (ToGA): a phase 3, open-label, randomised controlled trial. Lancet. 2010;376(9742):687-97.

[57]   Slamon DJ, Leyland-Jones B, Shak S, Fuchs H, Paton V, Bajamonde A, et al. Use of chemotherapy plus a monoclonal antibody against HER2 for metastatic breast cancer that overexpresses HER2. N Engl J Med. 2001;344(11):783-92.

[58]   Zuo Q, Liu J, Zhang J, Wu M, Guo L, Liao W. Development of trastuzumab-resistant human gastric carcinoma cell lines and mechanisms of drug resistance. Sci Rep. 2015;5:11634.

[59]   Gschwantler-Kaulich D, Tan YY, Fuchs EM, Hudelist G, Kostler WJ, Reiner A, et al. 2 PTEN expression as a predictor for the response to trastuzumab-based therapy in Her-2 overexpressing metastatic breast cancer. PLoS One. 2017;12(3):e0172911.

[60]   Fujita T, Doihara H, Kawasaki K, Takabatake D, Takahashi H, Washio K, et al. PTEN activity could be a predictive marker of trastuzumab efficacy in the treatment of ErbB2-overexpressing breast cancer. Br J Cancer. 2006;94(2):247-52.

[61]   Park BH, Davidson NE. PI3 kinase activation and response to Trastuzumab Therapy: what's neu with herceptin resistance? Cancer Cell. 2007;12(4):297-9.

[62]   Grohn P, Helle L, Numminen S, Heinonen E. Combination of carmofur and interferon-alpha-2B in advanced gastrointestinal cancer--a phase II pilot study. Acta Oncol. 1994;33(6):711-3.

[63]   Ito K, Yamaguchi A, Miura K, Kato T, Baba S, Matsumoto S, et al. Oral adjuvant chemotherapy with carmofur (HCFU) for colorectal cancer: five-year follow-up. Tokai HCFU Study Group--third study on colorectal cancer. J Surg Oncol. 1996;63(2):107-11.

[64]   Kajanti MJ, Pyrhonen SO. Phase II trial of oral carmofur in advanced pancreatic carcinoma. Ann Oncol. 1991;2(10):765-6.

[65]   Ito K, Yamaguchi A, Miura K, Kato T, Baba S, Matsumoto S, et al. Effect of oral adjuvant therapy with Carmofur (HCFU) for distant metastasis of colorectal cancer. Int J Clin Oncol. 2000;5(1):29-35.

[66]   Osterlund P, Elomaa I, Virkkunen P, Joensuu H. A phase I study of raltitrexed (Tomudex) combined with carmofur in metastatic colorectal cancer. Oncology. 2001;61(2):113-9.

[67]   Planchon SM, Waite KA, Eng C. The nuclear affairs of PTEN. J Cell Sci. 2008;121(Pt 3):249-53.

[68]   Vazquez F, Ramaswamy S, Nakamura N, Sellers WR. Phosphorylation of the PTEN tail regulates protein stability and function. Mol Cell Biol. 2000;20(14):5010-8.

[69]   Nakamura T, Ohno M, Tabuchi Y, Kamigaki T, Fujii H, Yamagishi H, et al. Optimal duration of oral adjuvant chemotherapy with Carmofur in the colorectal cancer patients: the Kansai Carmofur Study Group trial III. Int J Oncol. 2001;19(2):291-8.

[70]   Baehring JM, Fulbright RK. Delayed leukoencephalopathy with stroke-like presentation in chemotherapy recipients. J Neurol Neurosurg Psychiatry. 2008;79(5):535-9.

SUPPORTING INFORMASTION

[Insert supporting information here]

请提供研究身份识别材料，可通过另外的附件上传，具体详见附件《论文责任者（论文作者）研究身份识别材料》

Figure Legends

Figure 1. A. ECM-receptor interaction pathways and focal adhesion (FA) pathways are significant overrepresented in above 555 genes. B. THBS2 expression is extremely down-regulated in all digestive tract organs. C. THBS2 expression is significantly up-regulated in gastric tumors as compared to normal tissues in both our samples and TCGA study. D.THBS2 gene expression is higher in M1 samples in TCGA vs N0 (M0) and N3 (M0) samples. Note: TCGA, The Cancer Genome Atlas; KEGG, Kyoto Encyclopedia of Genes and Genomes.

Figure 2. A. Representative photos from immunohistochemical staining for THBS2 in GC (400×). B. Patients with higher THBS2 expression displayed a significantly shorter overall survival time, whereas patients with lower THBS2 expression showed a favorable prognosis (median 28.5 months vs. 40.5 months, P =0.00039). C. Variable importance for machine-learning algorithm model, scaled to a maximum of 1.0. (Variables that are not important will have small positive or negative values. The negative value does not necessarily reflect a negative risk, but indicates that there is no significant contribution).

Figure 3. A. Representative images of primary tumorspheres (P1, P3, P6 and P10). B. Western blotting showed the expression of THBS2 protein and PTEN protein in PGTCs and GES cells. C. Downregulation of THBS2 altered the pPTEN expression and inhibited the AKT activation in PGTCs. D. Downregulation of THBS2 inhibited the activation of FAK signaling in PGTCs. E. Downregulation of THBS2 increased expression of epithelial marker E-cadherin, but decreased expression of mesenchymal makers Vimentin and N-cadherin in PGTCs. F. Downregulation of THBS2 inhibited the migration of PGTCs. G. PGTCs generated 5.4 times more tumorispheres than PGTCsTHBS2-.

Figure 4. A. Cluster of differentially expressed genes in transcriptome data. B. Cluster of differentially expressed genes in proteome data. C. A Venn diagram shows the numbers of differentially expressed genes between proteome, transcriptome and GEO database. D. GSEA reveals global transcriptome differences in principal components after overexpression of THBS2 in NCI-N87 cells. E. Regulation_network: main regulation network of differentially expressed genes. The data were analyzed by combining the transcriptome, proteome and GEO data. Bright yellow highlighted the key regulators validated by western blotting; red and blue marked the up-regulated or down-regulated genes respectively; orange squares marked genes that were not significantly changed in transcriptome and proteome data; triangles marked the differentially expressed proteins; ellipses marked differentially mRNAs; arrows marked the differentially expressed genes in GEO database; diamond marked differentially expressed genes in both transcriptome and proteome data; parallelograms marked differentially expressed genes in both GEO and transcriptome data; squares marked differentially expressed genes in both GEO and proteome data; hexagons marked differentially genes in both transcriptome, proteome and GEO data. F. Validation of key proteins in the regulation network of THBS2 by Western blotting.

Figure 5. A. Nuclear protein 80 µg/lane, others 20 µg/lane. PTEN protein was mostly in the cytoplasm of PGTCs and NCI-N87 cells. B. After 48-h incubation with carmofur at different concentrations (0, 1, 3, 5 and 10 mM), protein expression of nuclear and cytoplasm PTEN was tested in both PGTCs and NCI-N87 cells. The most effective concentrations of carmofur for PGTCs and NCI-N87 cells were 3 mM and 5 mM, respectively. C. The cut-off point of trastuzumab concentration-effect line of PGTCs/carmofur came earlier than PGTCs (4 µg/ml vs 5 µg/ml). This was also found in the NCI-N87/carmofur cells as compared to NCI-N87 cells (3 µg/ml vs 5 µg/ml). D. Cells treated with carmofur at optimal concentrations (3 mM for PGTCs and 4 mM for NCI-N87 cells) for at least 48 h generated less tumorispheres than the untreated cells.

Figure 6. A. Orthotropic xenograft model: 2 out of 3 in the PGTCs group and 1 out of 3 in the NCI-N87THBS2+ group. Neither THBS2 knock-down nor carmofur treated groups had liver metastases. Liver metastases were identified in tissues after H&E staining. B. Subcutaneous xenograft model: in the NCI-N87 group, carmofur significantly reduced the tumor volume. The combination of carmofur and trastuzumab achieved the best tumor-inhibitory effect. C. In the NCI-N87THBS2+ group, carmofur failed to significantly reduce tumor volume. The combination of carmofur failed to improve the effect of trastuzumab. D. The final tumor

22

volumes (the 8th week) were compared between two groups. The tumor volume in the NCI-N87THBS2+ group was larger than in the NCI-N87 group.

Figures

Fig. 1

Fig. 2

A negative   0/1+   2+   3+

B

THBS — 0 — 1

P=0.00039

Number at risk

THBS					
86	74	46	20	2	
132	87	39	11	0	

C

AGE
SIZE
N
THBS
T
AFP
CEANA
BMI
CEA
CA199
HER2
AFPNA
CA199NA

Relative importance
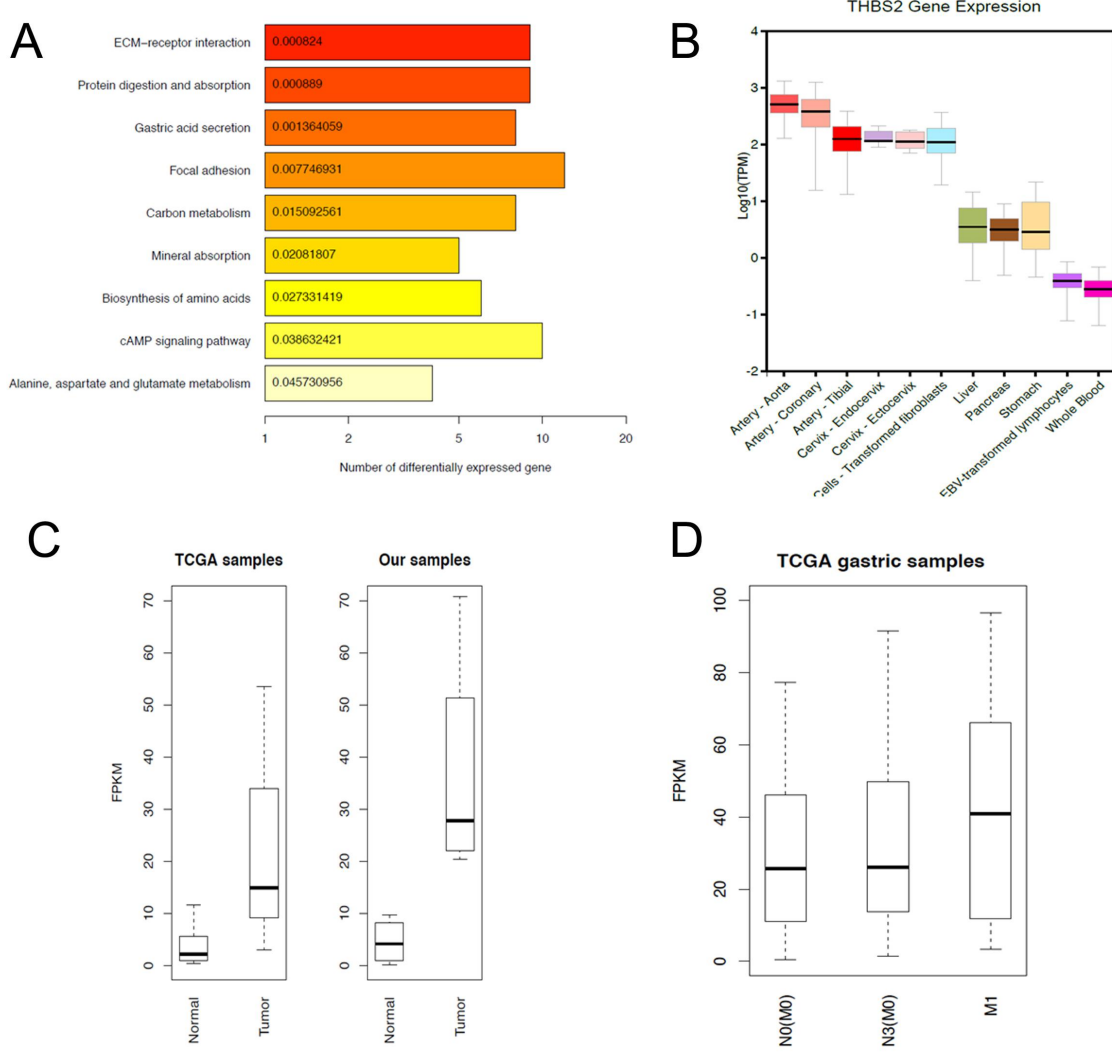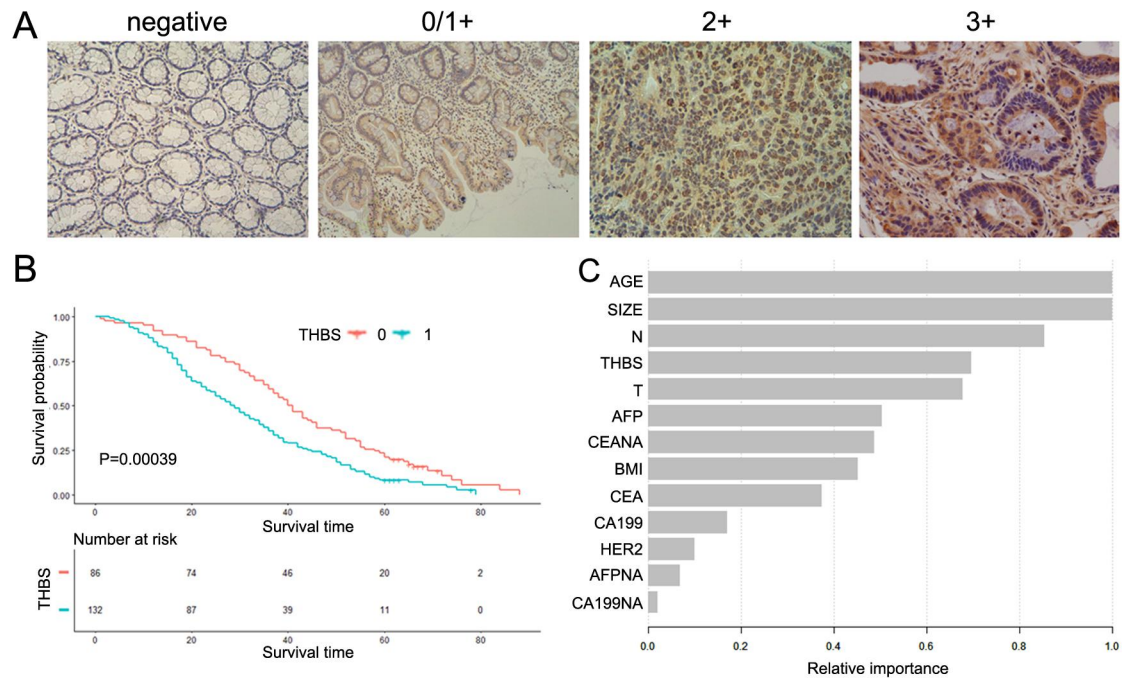
Fig. 3

Fig. 4

Fig. 5

Fig. 6

29
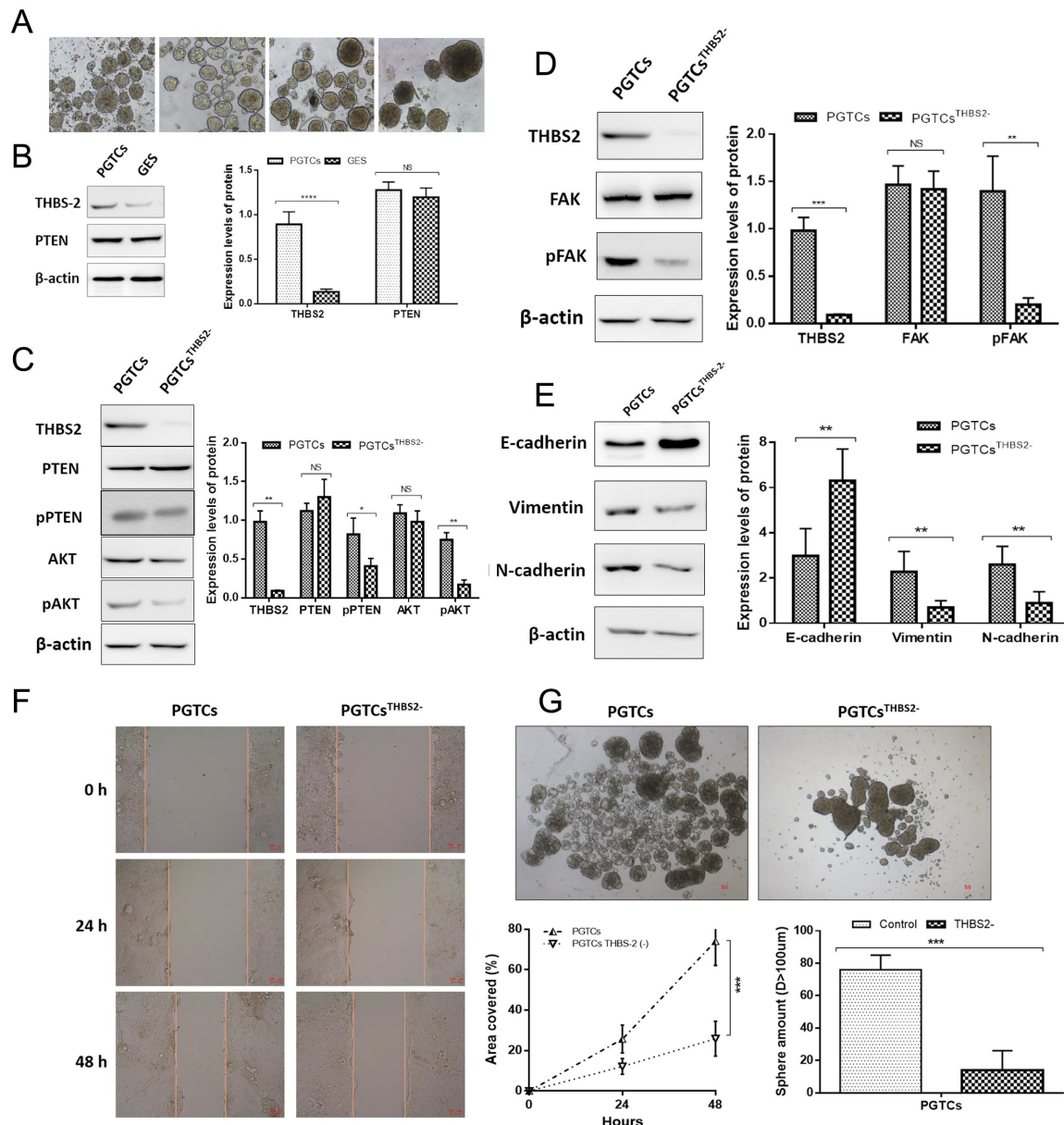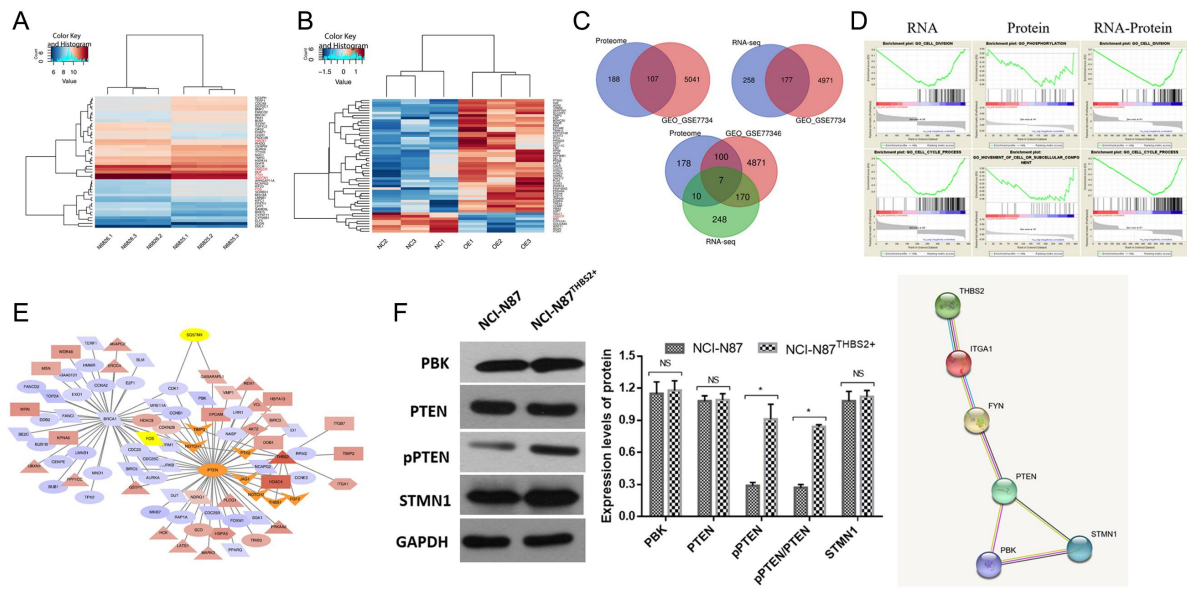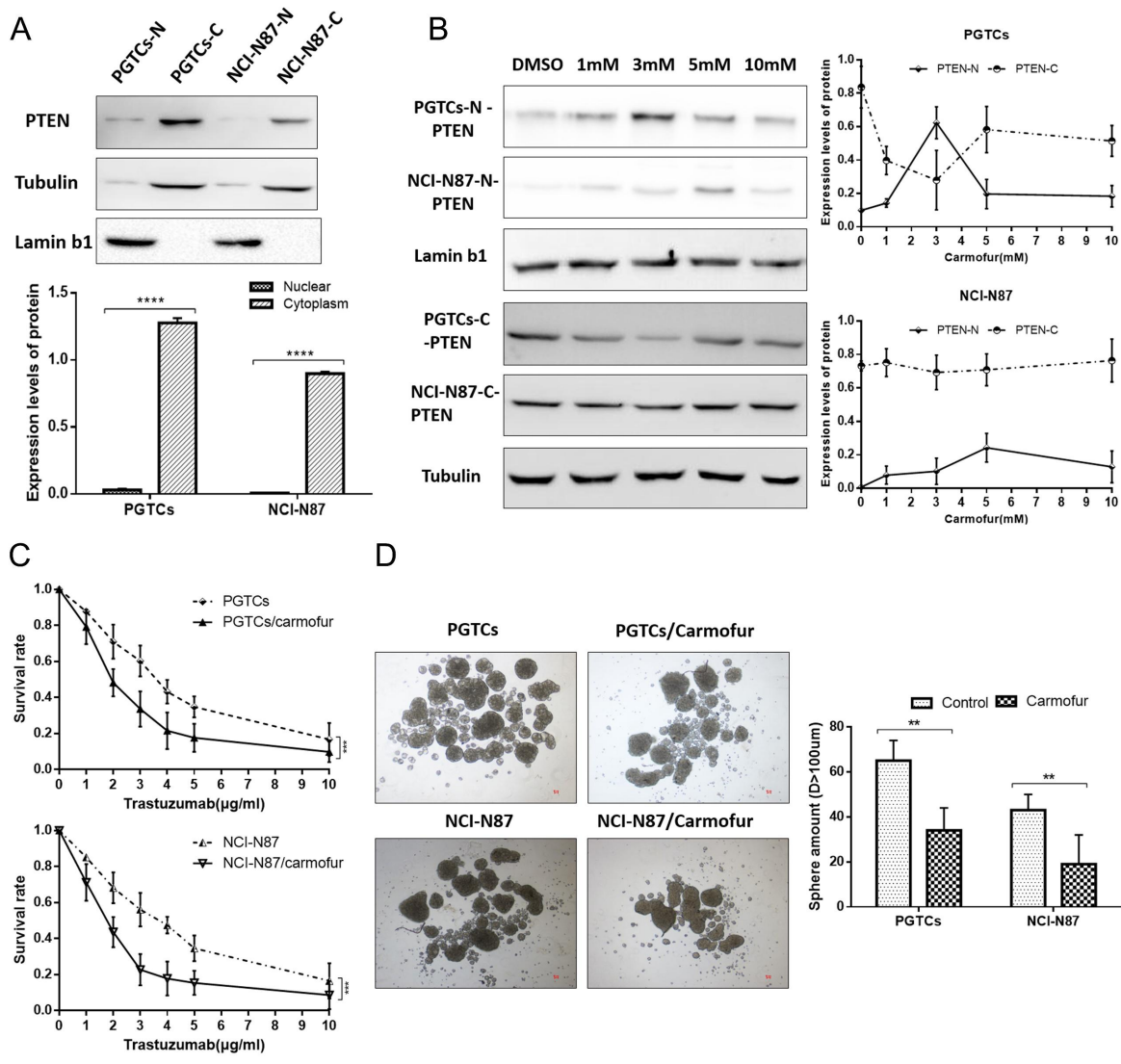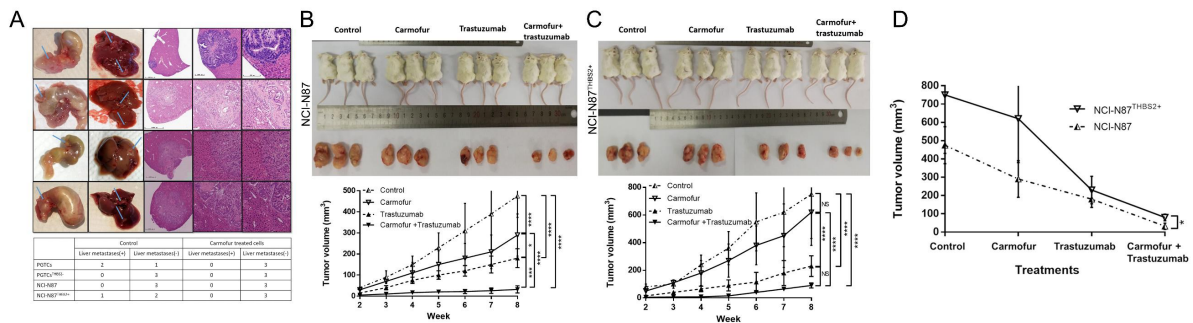
Tables

Table 1. Demographic and clinical characteristics of patients.

|	THBS2 (-) (n=86)	THBS2 (+) (n=132)	P	P*
Age (years)	60.59± 11.57	60.52 ± 12.38	0.963	0.810
Sex			0.539	-
Male	62 (72.09%)	90 (68.18%)		
Female	24 (27.91%)	42 (31.82%)		
BMI (kg/m2)	23.19 ± 3.04	22.61 ± 3.20	0.179	0.190
Tumor location			0.809	-
Upper	18 (20.93%)	22 (16.67%)		
Middle	15 (17.44%)	28 (21.21%)		
Lower	45 (52.33%)	71 (53.79%)		
Diffuse	8 (9.30%)	11 (8.33%)		
Size (cm)	5.60 ± 3.12	5.76 ± 2.58	0.675	0.480
Bormmann classification			0.164	-
Mass	10 (11.63%)	5 (3.79%)		
Ulcerative	45 (52.33%)	76 (57.58%)		
Infiltrative ulcerative	20 (23.26%)	31 (23.49%)		
Diffuse Infiltrative	11 (12.79%)	20 (15.15%)		
Differentiation			0.022	0.012
Well	2 (2.33%)	1 (0.76%)		
Moderately	26 (30.23%)	21 (15.91%)		
Poor or Signet-Ring	58 (67.44%)	110 (83.33%)		
T			0.073	-
T1	4 (4.65%)	1 (0.76%)		
T2	8 (9.30%)	5 (3.79%)		
T3	26 (30.23%)	39 (29.55%)		
T4	48 (55.81%)	87 (65.91%)		
N			0.018	-
N0	14 (16.28%)	13 (9.85%)		
N1	19 (22.09%)	19 (14.39%)		
N2	21 (24.42%)	22 (16.67%)		
N3	32 (37.21%)	78 (59.09%)		
M			0.027	0.028
M0	83 (96.51%)	116 (87.88%)		
M1	3 (3.49%)	16 (12.12%)		
Metastasis sites			0.095	
None	83 (96.51%)	116 (87.88%)		
Liver	0	7 (5.30%)		
Lung	2 (2.33%)	2 (1.52%)		
Peritoneal	1 (1.16%)	4 (3.03%)		
Multiple	0	3 (2.27%)		
HER2			0.114	-

-	34 (39.54%)	39 (29.55%)		
+	30 (34.88%)	54 (40.91%)		
++	22 (25.58%)	33 (25.00%)		
+++	0	6 (4.55%)		
CEA (ug/l)	20.04 ± 67.43	10.27 ± 33.41	0.253	0.125
AFP (ug/l)	4.36 ± 13.76	60.63 ± 500.74	0.407	0.612
CA19-9 (u/ml)	126.95 ± 443.68	155.57 ± 1025.75	0.844	0.831

Note: T, T stage, depth of invasion; N, N stage, lymph node metastasis; M, M stage, distant metastases. BMI: body mass index. Continuous variables: Mean ± SD, P - Student's t test, P* - Kruskal Wallis Test.

Binomial and categorical variables: N (%), P - Pearson's χ2, P* - Fisher's exact tests.

Univariate analysis was employed to explore the relationship between THBS2 expression and postoperative long-term survival (longer than 5 years) (Table 2). Results showed that BMI (P=0.030), stage T4 (P=0.004), stage N3 (P=0.005) and THBS2 expression (P=0.003) were associated with postoperative survival time longer than 5 years. Furthermore, the machine-learning algorithm model was developed to quantify the relative importance of each variable related to postoperative long-term survival (Fig. 2c and Table 3). The relative contribution of THBS2 to the long-term survival was up to 0.695 (Table 3).

Table 2. Univariate analysis for 5-year survival

	Statistics	5-year survival	
		OR (95%CI)	P
Age (years)	60.55 ± 12.04	1.03 (0.99, 1.06)	0.139
Sex			
Male	152 (69.73%)	1.0	
Female	66 (30.28%)	0.51 (0.20, 1.30)	0.159
BMI (kg/m2)	22.84 ± 3.14	1.15 (1.01, 1.30)	0.030
Tumor location			
Upper	40 (18.35%)	1.0	
Middle	43 (19.72%)	0.41 (0.11, 1.49)	0.175
Lower	116 (53.21%)	0.74 (0.29, 1.85)	0.513
Diffuse	19 (8.72%)	0.22 (0.03, 1.92)	0.172
Size (cm)	5.70 ± 2.80	1.06 (0.93, 1.20)	0.398
Bormmann			
Mass	15 (6.88%)	1.0	
Ulcerative	121 (55.51%)	2.77 (0.35, 22.30)	0.338
Infiltrative ulcerative	51 (23.39%)	1.87 (0.21, 16.85)	0.578
Diffuse Infiltrative	31 (14.22%)	2.07 (0.21, 20.37)	0.531
Differentiation			
Well	3 (1.38%)	1.0	
Moderately	47 (21.56%)	0.47 (0.04, 5.82)	0.559
Poor or Signet-Ring	168 (77.06%)	0.29 (0.03, 3.29)	0.315
T			
T1	5 (2.29%)	1.0	
T2	13 (5.96%)	0.20 (0.02, 1.82)	0.153
T3	65 (29.82%)	0.17 (0.03, 1.10)	0.063
T4	135 (61.93%)	0.07 (0.01, 0.43)	0.004
N			
N0	27 (12.39%)	1.0	
N1	38 (17.43%)	0.76 (0.24, 2.43)	0.646
N2	43 (19.72%)	0.76 (0.24, 2.35)	0.629
N3	110 (50.46%)	0.19 (0.06, 0.61)	0.005
M			
M0	199 (91.28%)	1.0	
M1	19 (8.72%)	1.15 (0.31, 4.19)	0.838
Chemotherapy			
No	58 (26.61%)	1.0	
Yes	160 (73.39%)	0.73 (0.32, 1.65)	0.443
THBS2			
-	86 (39.45%)	1.0	
+	132 (60.55%)	0.30 (0.14, 0.66)	0.003
HER2			
-	73 (33.49%)	1.0	
+	84 (38.53%)	0.93 (0.40, 2.19)	0.869

++	55 (25.23%)	0.51 (0.17, 1.54)	0.231
+++	6 (2.75%)	1.02 (0.11, 9.50)	0.988
CEA (μg/l)	14.12 ± 49.69	0.99 (0.97, 1.02)	0.616
AFP (μg/l)	38.52 ± 390.33	0.83 (0.52, 1.33)	0.444
CA19-9 (U/ml)	144.21 ± 841.92	0.99 (0.97, 1.01)	0.310

Note: OR: odds ratio, 95% CI: confidence interval. BMI: body mass index. T: T stage, depth of invasion; N: N stage, lymph node metastasis; M: M stage, distant metastases. Continuous variables: Mean ± SD. Binomial and categorical variables: N (%).

Table 3. Variable importance for 5-year survival

Feature	Gain	Cover	Frequency	Relative importance
Age (years)	0.156	0.173	0.183	1.000
Size (cm)	0.156	0.163	0.165	0.999
N	0.133	0.086	0.073	0.854
THBS2	0.109	0.070	0.064	0.695
T	0.106	0.097	0.083	0.677
AFP (µg/l)	0.079	0.097	0.101	0.503
BMI (kg/m2)	0.071	0.099	0.110	0.452
CEA (µg/l)	0.058	0.109	0.119	0.374
CA19-9 (U/ml)	0.027	0.018	0.018	0.171
HER2	0.016	0.017	0.018	0.100

Note: T, T stage, depth of invasion; N, N stage, lymph node metastasis; M, M stage, distant metastases. BMI: body mass index.